FEBS Letters 587 (2013) 3968–3972

FEBS Letters

journal homepage: www.FEBSLetters.org

Structure of the (*E*)-4-hydroxy-3-methyl-but-2-enyl-diphosphate reductase from *Plasmodium falciparum*

Ingo Rekittke [a], Elena Olkhova [b], Jochen Wiesner [a], Ulrike Demmer [b], Eberhard Warkentin [b], Hassan Jomaa [a,*], Ulrich Ermler [b,*]

[a] Medizinische Klinik IV (Hämatologie), Justus-Liebig-Universität Giessen, Klinikstrasse 33, D-35392 Giessen, Germany
[b] Max-Planck-Institut für Biophysik, Max-von-Laue-Straße 3, D-60438 Frankfurt am Main, Germany

ARTICLE INFO

Article history:
Received 6 September 2013
Revised 15 October 2013
Accepted 20 October 2013
Available online 1 November 2013

Edited by Stuart Ferguson

Keywords:
Isoprenoid biosynthesis
LytB
X-ray structure
Drug design
Plasmodium falciparum

ABSTRACT

Terpenoid precursor biosynthesis occurs in human and many pathogenic organisms via the mevalonate and 2-*C*-methyl-D-erythritol-4-phosphate (MEP) pathways, respectively. We determined the X-ray structure of the Fe/S containing (*E*)-4-hydroxy-3-methyl-but-2-enyl-diphosphate reductase (LytB) of the pathogenic protozoa *Plasmodium falciparum* which catalyzes the terminal step of the MEP pathway. The cloverleaf fold and the active site of *P. falciparum* LytB corresponds to those of the *Aquifex aeolicus* and *Escherichia coli* enzymes. Its distinct electron donor [2Fe–2S] ferredoxin was modeled to its binding site by docking calculations. The presented structural data provide a platform for a rational search of anti-malarian drugs.

1. Introduction

Malaria is considered as one of the world's leading causes of morbidity and mortality with annually over 500 million symptomatic infections and 1 million lethal cases [1]. Infections to humans are caused by parasitic protozoa of the genus *Plasmodium* that is subdivided into the four pathogenic species *Plasmodium falciparum*, *Plasmodium vivax*, *Plasmodium ovale* and *Plasmodium malariae*. *P. falciparum*, the causative agent of malignant tertian malaria (malaria tropica), is the most dangerous among them and responsible for the majority of the lethal cases [1]. As *P. falciparum* increasingly developes resistances against commonly used drugs for therapeutic and prophylactic purposes [2] identification of novel targets for finding anti-malarial agents is of prime importance.

Terpenoids such as dolichols, quinones, carotenoids, vitamins and sterols, are involved in vital metabolic processes in all kingdoms of life. Despite their great diversity with over 35 000 distinct compounds, all terpenoids are derived from the two 5-carbon isoprene precursors isopentenyl diphosphate (IPP) and dimethylallyl diphosphate (DMAPP). Interestingly, nature has evolved two distinct pathways for their biosynthesis: the mevalonate and the 2-*C*-methyl-D-erythritol-4-phosphate (MEP) pathways. Animals, fungi, archaea and some bacteria use the well-known mevalonate pathway, the vast majority of bacteria and some parasitic protozoa of the phylum Apicomplexa, the MEP pathway [3–5]. Since the MEP pathway is not used by humans, it is considered as an attractive target for the development of new antimicrobial agents, in particular, drugs against the parasitic protozoa *Plasmodium*, responsible for the malaria disease [6–9]. Enzymes of the MEP pathways have been thoroughly explored in the last 20 years with respect to their molecular and functional properties [10]. The terminal enzyme of the MEP pathway, (*E*)-4-hydroxy-3-methyl-but-2-enyl-diphosphate reductase (LytB/IspH) converts (*E*)-4-hydroxy-3-methyl-but-2-enyl-diphosphate (HMBPP) into IPP and DMAPP (Fig. 1) [11]. LytB was characterized as [4Fe–4S] carrying monomeric or dimeric enzyme with of a molecular mass of 30–35 kDa per monomer. X-ray structures were recently determined for the *Aquifex aeolicus* and *Escherichia coli* enzymes; the latter in complex with substrate and products. On this basis a structure-based mechanism could be postulated and inhibition studies initiated [12–15].

Abbreviations: LytB, (*E*)-4-hydroxy-3-methyl-but-2-enyl-diphosphate reductase; MEP, 2-*C*-methyl-D-erythritol-4-phosphate; MEcPP, 2-*C*-methyl-D-erythritol-2,4-cyclo-diphosphate; HMBPP, (*E*)-4-hydroxy-3-methyl-but-2-enyl-diphosphate; IPP, isopentenyl diphosphate; DMAPP, dimethylallyl diphosphate

* Corresponding authors. Fax: +49 641 9941509 (H. Jomaa), +49 69 63031002 (U. Ermler).

E-mail addresses: hassan.jomaa@uniklinikum-giessen.de (H. Jomaa), ulrich.ermler@biophys.mpg.de (U. Ermler).

0014-5793/$36.00
http://dx.doi.org/10.1016/j.febslet.2013.10.029

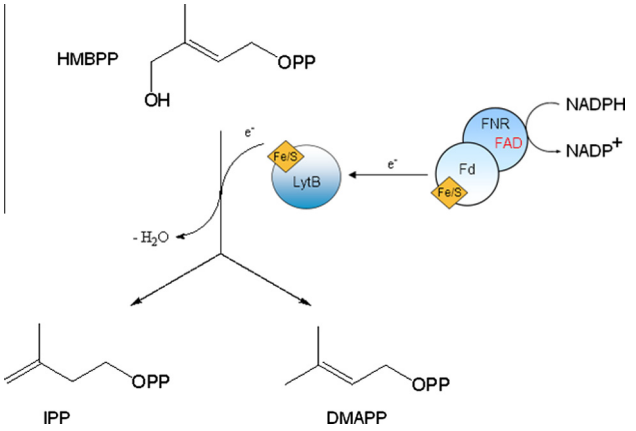

Fig. 1. Reaction of LytB which converts HMBPP into IPP or DMAPP. Electrons to the [4Fe–4S] cluster of LytB are supplied in *P. falciparum* by the ferredoxin/ferredoxin-$NADP^+$ reductase system. NADPH transfers a hydride to FAD that conducts two times one electron to a [2Fe–2S] cluster of ferredoxin and further to the [4Fe–4S] cluster of LytB.

In this report we describe the structure, and the potential substrate and electron donor binding sites of LytB of *P. falciparum*, the direct target for drug developments against the major pathogenic malaria parasite.

2. Materials and methods

2.1. Enzyme production

TOP 10 *E. coli* cells (Invitrogen) were transformed with the pASKPfalLytB vector containing His_6-tagged LytB and grown in LB-broth medium (Roth) supplemented with 150 μg ml^{-1} ampicillin and 300 μM $FeCl_3$ at 37 °C [16]. The cells were harvested by centrifugation (17700×g, 15 min, 4 °C) and stored at −30 °C until further use. All subsequent steps were carried out under oxygen exclusion. The cell pellet (30 g) was resuspended in 300 ml 30 mM Tris–HCl (pH 7.5), 150 mM NaCl, 15 mM imidazole and lysed by ultrasonic treatment at 0 °C. Purification was performed using Co-TALON, Source 15S and Superdex 200 columns as described in detail in the Supplementary data. LytB was stored at a concentration of ca. 12 mg ml^{-1} in 30 mM Tris–HCl (pH 7.5) and 150 mM NaCl.

2.2. Crystallization and X-ray structure analysis

Crystallization was performed at 18 °C in an anaerobic tent (95% N_2, 5% H_2) using the sitting drop vapour diffusion method. Best crystals grew by mixing 2.0 μl enzyme solution (12 mg ml^{-1} LytB, 30 mM Tris–HCl, 150 mM NaCl, pH 7.5) and 1.0 μl reservoir solution composed of 30% w/v PEG 4000, 100 mM sodium citrate (pH 5.6) and 100 mM ammonium sulfate. Data were collected at the Swiss-Light source beamline PXII and processed with XDS [17]. The structure was determined with the multiple anomalous dispersion method using the iron of the Fe/S cluster as anomalous scatterer. The iron positions were detected with SHELXD [18] and the phases calculated with SHARP [19]. After phase improvement with SOLOMON [20] a polypeptide model could be built in COOT [21] using the known LytB structures [12,13]. The structure was refined with REFMAC5 [22]. Crystal parameters, data collection and refinement statistics are listed in Table 1. Figs. 1–3 were produced with PYMOL (Schrödinger, LLC]. The atomic coordinates and the structure factor of LytB have been deposited in the Protein Data Bank, www.pdb.org with the ID code 4N7B.

2.3. Docking calculations

Fully unbiased protein–protein docking calculations on the basis of the determined LytB structure and the known ferredoxin structure from *P. falciparum* (PDB: 1iue) were performed with the molecular simulations software ICM-Pro (Molsoft LLC, La Jolla, CA) [23]. We calculated the size of the surface area buried at the interface, the number of hydrophobic contacts, binding energies, and overall electrostatic complementarities and reduced the generated number of LytB–ferredoxin complexes by defining a maximal distance between the redox centers involved in inter-protein electron transfer. A number of scripts were written to calculate interatomic distances, angles and torsion angles, as well as to evaluate the binding energies of the generated complexes. The most promising docking complexes were chosen and further refined by energy minimization and side chain optimization procedures. The software ICM-ODA (optimal docking area) [24] was used to determine the surface section of LytB that is most suitable to form an interface with another protein.

3. Results and discussion

3.1. Structure of LytB of P. falciparum

Recombinantly produced His_6-tagged LytB enzyme from *P. falciparum* was crystallized under anaerobic conditions. Its structure was determined by the multiple anomalous dispersion method and refined to final R/R_{free} factors of 17.5/19.5% at 2.2 Å resolution (Table 1).

In accordance to previous solution data [16] *P. falciparum* LytB was found like *E. coli* LytB as a monomer in contrast to the dimeric *A. aeolicus* LytB. *P. falciparum* LytB is essentially composed of three related α/β-domains (domains A–C) arranged in a cloverleaf form with the Fe/S-cluster in its center (Fig. 2; Supplementary Fig. 1A). This architecture corresponds to that of *A. aeolicus* and *E. coli* LytB [12,13]. In contrast to the *A. aeolicus* enzyme, the *P. falciparum* and *E. coli* enzymes contain a C-terminal extension fused to helix α4c. After a turn it linearly spans over the entire domain C and is partly associated as a strand to the central four-stranded parallel β-sheet. Subsequently, the C-terminal extension passes the backside of the Fe/S cluster and continues to the top of domain A. In contrast to *E. coli* LytB the terminal residues of the *P. plasmodium* enzyme are folded as an α-helix (α1D) which is attached to helix α1A (Fig. 2A). Superposition between the different LytB structures with DALI [25] results in an rms deviation of 3.0 Å between *P. falciparum* and *A. aeolicus* LytB (sequence identity 32%) and of 1.4 Å between *P. falciparum* and *E. coli* LytB (sequence identity 40%).

This higher similarity between the latter enzymes is mainly due to a large-scale conformational change of the variable domain C (Fig. 2B). *A. aeolicus* LytB is crystallized in an open state [12] whereas *P. falciparum* and *E. coli* LytB in a closed state [13]. Open-to-close transition implicates a rotation of domain C towards the active site crevice. Interestingly, domain C of *E. coli* LytB is rotated ca. 10° further down to the active site crevice than domain C of *P. falciparum* LytB resulting in displacements at its top up to 5 Å. Further significant deviations up to 5 Å between the known LytB structures are only found in the loops following helices α2B, α3B and α4C. The loop following helix α1A is conformationally distinct between *A. aeolicus* and *P. falciparum*/*E. coli* LytB. These differences do, however, not affect the active site structure.

3.2. The Fe/S-cluster and the catalytic site

The *P. falciparum* LytB crystal structure exhibits an inactive [3Fe–4S] cluster already observed in *A. aeolicus* and most *E. coli* LytB structures [12,13]. The three iron atoms are ligated to three

Table 1
Data collection and refinement statistics.

Data set	Native	Peak	Inflection	Remote
Data collection				
Wavelength (Å)	0.92	1.7382	1.7406	1.7141
Space group	$P3_121$	$P3_121$	$P3_121$	$P3_121$
Resolution (Å)	2.2–50.0 (2.2–2.3)	2.4–50.0 (2.4–2.5)	2.6–50.0 (2.6–2.7)	2.6–50.0 (2.6–2.7)
Cell axis (Å)	116.1, 77.0	115.8, 76.8	115.9, 76.6	115.6, 76,8
Completeness (%)	99.5 (99.8)	99.6 (99.2)	99.6 (99.3)	99.7 (99.3)
R_{sym} (%)	8.9 (79.5)	7.4 (69.3)	6.9 (45.4)	8.4 (38.2)
I/sig$I$	15.5 (5.5)	14.1 (3.0)	17.3 (4.4)	14.5 (5.0)
Redundancy	6.0 (6.0)	5.5 (5.0)	4.9 (4.8)	4.9 (4.9)
Refinement statistics				
No. of mon. in a.u.	1			
No. of residues, [4Fe–4S] clusters, solvents in a.u.	318, 1, 189			
Resolution (Å)	2.2–50.0 (2.26–2.20)			
$R_{working}$, R_{free} (%)	17.5, 19.5 (26.0, 27.9)			
$B_{average}$ (polypeptide, [4Fe–4S] cluster, solvent) (Å^2)	45.6, 26.4, 44.6			
R.m.s. deviation bond lengths (Å)	0.009			
Bond angles (°)	1.45			

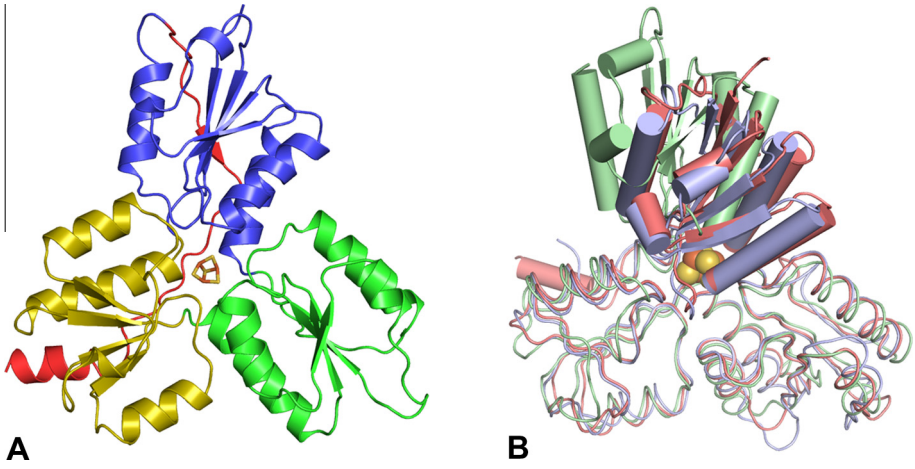

Fig. 2. Structure of *P. falciparum* LytB. (A) Monomeric LytB is composed of three α/β-domains (domain A: yellow; domain B: green; domain C: blue) and a C-terminal extension (red). The central [3Fe–4S]-cluster is fixed by cysteines from all three domains. (B) Alignment of the domains A and B core of *P. falciparum* (red), E. coli (blue) and *A. aeolicus* LytB (green). Domain C of *P. falciparum* and *E. coli* LytB is rotated towards the frontside of the active site forming a closed conformation; domain C of *A. aeolicus* LytB is in an open conformation.

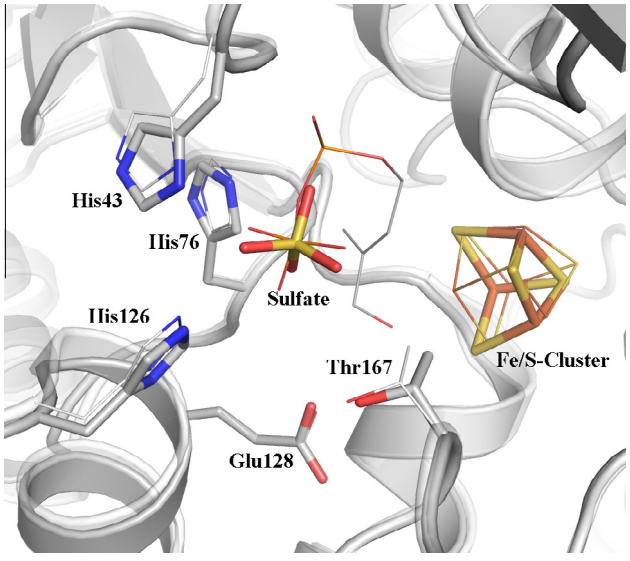

Fig. 3. Active site of *P. falciparum* LytB (stick model) and *E. coli* LytB–HMPBB complex (line model). The Fe/S cluster and crucial residues for substrate binding and catalysis are superimposed showing their high similarity.

strictly conserved cysteines (Cys14, Cys98 and Cys196) that protrude from each of the domains and thus link them together. The complete [4Fe–4S] cluster contains a non-cysteine bound iron that points towards bulk solvent [14] and becomes readily dissociated during the crystallization process. The substrate binding site is located in front of the iron-sulfur cluster inside a crevice that is formed by loops following strands β1 (β1A, β1B, β1C), β3 and 4 (Fig. 2A, Supplementary Fig. 1A). The accurate binding of the substrate HMBPP and its conformation is known from the LytB–HMBPP complex of *E. coli* [14].

The active site appears to be formed by an open-to-close transition process triggered by substrate binding. Domain C is rotated towards the front of the molecule and thus encapsulates the Fe/S cluster and the active site against bulk solvent (Fig. 2B). The closed conformation of *P. falciparum* LytB is presumably induced by a sulfate molecule positioned at the β-phosphate binding site of HMBPP found in the *E. coli* LytB–HMBPP complex (Fig. 3) [14]. (The precipitant solution contains 100 mM ammonium sulfate). The different position of domain C relative to the core (domain A+B) (Fig. 2B) in *E. coli* and *P. falciparum* LytB might be due to structural differences between diphosphate (or HMBPP) and sulfate, respectively, to sequence differences between the two LytB or to crystal lattice effects that, in particular, influence the flexible domain C.

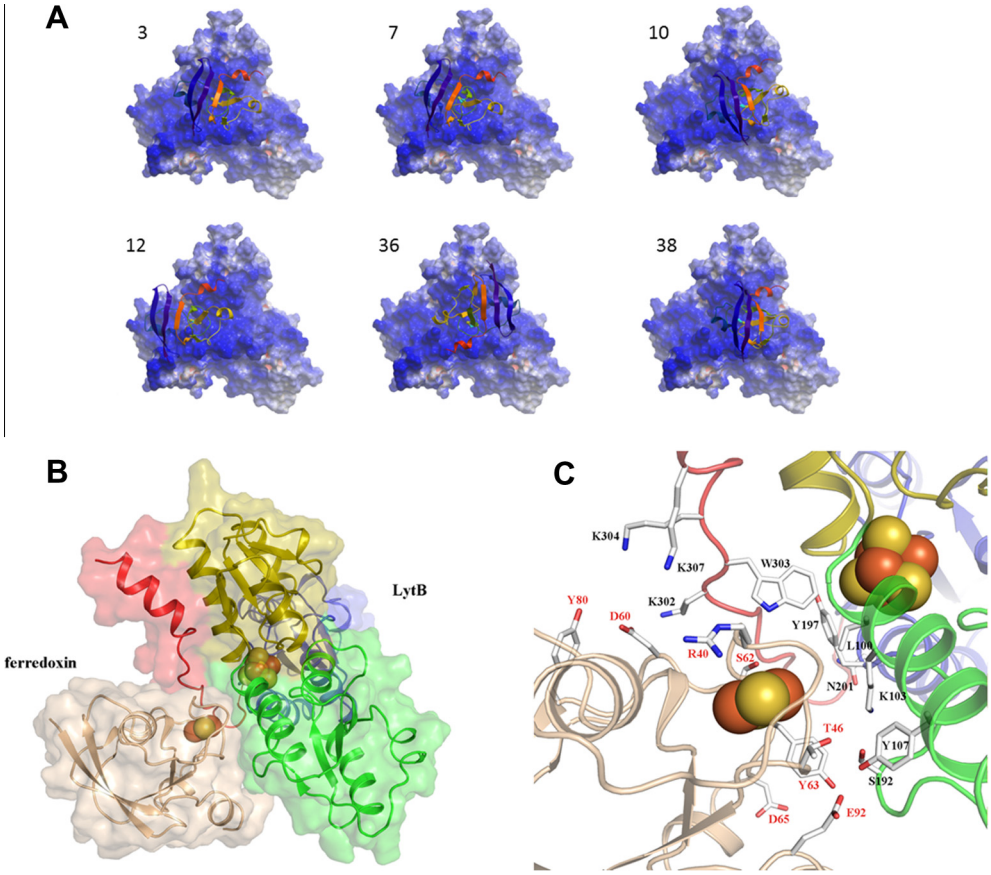

Fig. 4. Plausible complexes between LytB and ferredoxin from *P. falciparum* generated by protein–protein docking calculations (ICM-Pro, Molsoft). (A) The six energetically most favorable LytB–ferredoxin complexes are presented with LytB in a molecular surface and ferredoxin in a Ribbon representation. Negative electrostatic surface potentials for LytB are shown in red, positive ones in blue. (B) The interface between LytB and ferredoxin. The ferredoxin is colored in wheat, domains A–C of LytB in yellow, green and blue, the C-terminal extension in red, and Fe and S of the Fe/S cluster as orange and yellow spheres. (C) Detailed interactions between LytB and ferredoxin. Side chains are shown as sticks. The formation of only few specific polar interactions between LytB and ferredoxin, according to the docking calculations performed, is compatible with the physiological requirement for a rather weak protein–electron donor complex.

Independent of the exact position of domain C, the strictly conserved residues His43, His76, His126, Glu128 and Thr97 involved in substrate binding are found in a virtually identical conformation and position in *P. falciparum* and *E. coli* LytB documented by an rms deviation of <0.5 Å. (Fig. 3). While the surrounding of the methylbutenyl binding site of HMBPP including Thr97 and Glu128 is nearly identical, that of the diphosphate indicates a few minor differences in the second interaction shell. For example, Ser226 of a serine cluster (Ser226, Ser228 and Ser268) in *E. coli* LytB interacts with the β-phosphate of HMBPP and is hydrogen-bonded to the Asn229 side chain [14]. The equivalent Lys228 of *P. falciparum* LytB is directed to bulk solvent. Moreover, Ser228 of *E. coli* LytB involved in α-phosphate binding of HMBPP is replaced by an alanine in *P. falciparum* LytB. Differences are also found in the loop following strand β1A that is stabilized in *P. falciparum* LytB by a pronounced salt bridge between Lys40 and Asp45. Notably, His39 is turned towards His43 in the *P. falciparum* LytB and in the *E. coli* Lytb-PP_i structures but not in the *E. coli* LytB–HMBPP structure [14]. The found high degree of structural conservation among the LytB family members (Fig. 3, Supplementary Fig. 1B) clearly argue for a virtually identical substrate binding mode and catalytic mechanism best studied for the *E. coli* enzyme [14]. Therefore the combined information of the *P. falciparum* and *E. coli* LytB structures provide a serious platform for designing knowledge-based substrate inhibitors on a rational basis.

3.3. Putative binding of the electron donor [2Fe–2S] ferredoxin

Biochemical studies revealed that *P. falciparum* uses the ferredoxin/ferredoxin-$NADP^+$ reductase system for donating electrons to the [4Fe–4S] cluster of LytB (Fig. 1). They further demonstrated that LytB and a [2Fe–2S] ferredoxin form in vitro at low salt concentrations a relatively stable complex [16]. Since most organisms including *E. coli* and presumably *A. aeolicus* use the flavodoxin/flavodoxin-$NADP^+$ reductase system [26] as electron donor for LytB, the LytB–ferredoxin interface offers a very specific target for developing inhibitors for *P. falciparum* LytB. The contact region and the specific interactions between LytB and ferredoxin are, however, not structurally established which prompted us to perform in silico docking studies.

Qualitative protein surface analysis of LytB suggested the binding site for ferredoxin on its backside because only then a realistic distance for an effective electron transfer (13–14 Å) between the [4Fe–4S] and the [2Fe–2S] clusters can be adjusted without interfering with the catalytic site (Fig. 4). Ferredoxin might attach to a shallow well formed by the C-terminal extension, helix α1B and the loops after strands β4A and β4B. These assumption was confirmed by unbiased docking calculations using the ICM-Pro software [23]. Ca. 21 000 hits were generated; 31 of them remained when permitting only distances between [4Fe–4S] cluster of LytB and [2Fe–2S] cluster of ferredoxin of ⩽13 Å and energy scores

$\leqslant -20$ kcal/mol. The six LytB–ferredoxin complexes with the lowest energy are examined in detail (Fig. 4A, Supplementary Table 1).

In the best solutions the LytB–ferredoxin interfaces are very similar and only distinguished by the rotation angle between LytB and ferredoxin around an axis that links the two iron–sulfur clusters of both proteins. In complexes 3 and 7 LytB and ferredoxin adopt a similar orientation, whereas, in comparison, in complex 36 they are rotated by $\sim 180^\circ$ around the mentioned axis. Complexes 10, 12 and 38 moderately deviate from complex 3 (Fig. 4A). Optimal Docking Area (ODA) calculations [24], that determine the most likely docking site to another protein without applying distance restraints result in the same solution as the docking simulations (Supplementary Fig. 2). However, a clear top candidate (if one exists) under the best docking solutions was not detectable which might be possible with extensive molecular dynamics simulations to optimize the intermolecular contacts and, of course, by a crystal structure of the LytB–ferredoxin complex. The most probable candidate according to the current data is the LytB–ferredoxin complex 3 (Fig. 4). It forms the maximal number of specific hydrogen bonds and exhibits the lowest energy score value (−36.5 kcal/mol) which is the third best value of all ca. 21 000 LytB-ferredoxin complexes calculated without distance restraints.

In the best solutions the protein–protein contact is essentially accomplished by the same residues including Leu100, Lys103, Tyr107, Ser192, Tyr197, Asn201, Lys302, Trp303, Lys304, Lys307 of LytB and Arg40, Thr46, Ser62, Tyr63, Asp60, Asp65, Tyr80, Glu92 of ferredoxin (Fig. 4B+C). It becomes obvious that the C-terminal extension – if present – plays a crucial role in ferredoxin binding. Segment 37–46 of ferredoxin that envelops and thereby shields the [2Fe–2S] cluster is embedded into the shallow well. Residues Ser38, Ser43, Thr46, Ser 62, and Tyr63 of ferredoxin form an extended hydrophobic contact with Pro99, Leu100, Lys103, Tyr107, Ser192, Pro301 and Trp303 of LytB. A key role in electron transfer is attributed to Trp303 which is located in all docked LytB–ferredoxin complexes between the iron–sulfur clusters and is frequently in van der Waals contact to them. Trp303 sandwiched between Pro99 and Pro301, is projected towards bulk solvent in LytB and shielded after ferredoxin binding (Fig. 4C). It is also directly neighbored to Tyr197, the residue calculated in ODA to be most likely involved in the LytB–protein interface. A comparison between the C-terminal extensions of *P. falciparum* and *E. coli* LytB in the electron donor binding region revealed an rms deviation of 2.5 Å for the backbone atoms and only a moderate conservation of the side chains. Val300, Pro301, Lys302, Trp303 and Lys304 are exchanged to asparagine, isoleucine, valine, phenylalanine and glutamate. Substantial differences between the two enzymes are also found in other segments forming the assumed ferredoxin binding site (Supplementary Fig. 3). One example is the loop following strand β4B (Fig. 4C) which is displaced ca. 5 Å in *P. falciparum* compared to *E. coli* LytB.

Acknowledgements

This work was supported by the Else Kröner-Fresenius-Stiftung and the Max-Planck Society. We thank Hartmut Michel for continuous support and the staff of the PXII beamline at the Swiss Light Source (Villigen) for help during data collection.

Appendix A. Supplementary data

Supplementary data associated with this article can be found, in the online version, at http://dx.doi.org/10.1016/j.febslet.2013.10.029.

References

[1] WHO: World Malaria Report 2010.
[2] Rosenthal, P.J. and Miller, L.H. (2001) The need for new approaches to antimalarial chemotherapy. Antimalarial Chemother. 82, 3–13.
[3] Rohmer, M., Knani, M., Simonin, P., Sutter, B. and Sahm, H. (1993) Isoprenoid biosynthesis in bacteria: a novel pathway for the early steps leading to isopentenyl diphosphate. Biochem. J. 295, 517–524.
[4] Eisenreich, W., Bacher, A., Arigoni, D. and Rohdich, F. (2004) Biosynthesis of isoprenoids via the non-mevalonate pathway. Cell. Mol. Life Sci. 61, 1401–1426.
[5] Rohmer, M. (2008) From molecular fossils of bacterial hopanoids to the formation of isoprene units: discovery and elucidation of the methylerythritol phosphate pathway. Lipids 43, 1095–1107.
[6] Singh, N., Cheve, G., Avery, M.A. and McCurdy, C.R. (2007) Targeting the methyl erythritol phosphate (MEP) pathway for novel antimalarial, antibacterial and herbicidal drug discovery: inhibition of 1-deoxy-D-xylulose-5-phosphate reductoisomerase (DXR) enzyme. Curr. Pharm. Des. 13, 1161–1177.
[7] Wiesner, J., Reichenberg, A., Heinrich, S., Schlitzer, M. and Jomaa, H. (2008) The plastid-like organelle of apicomplexan parasites as drug target. Curr. Pharm. Des. 14, 855–871.
[8] Jomaa, H. et al. (1999) Inhibitors of the non-mevalonate pathway of isoprenoid biosynthesis as antimalarial drugs. Science 285, 1573–1576.
[9] Wiesner, J., Hintz, M., Altincicek, B., Sanderbrand, S., Weidemeyer, C., Beck, E. and Jomaa, H. (2000) *Plasmodium falciparum*: detection of the deoxyxylulose 5-phosphate reductoisomerase activity. Exp. Parasitol. 96, 182–186.
[10] Grawert, T., Groll, M., Rohdich, F., Bacher, A. and Eisenreich, W. (2011) Biochemistry of the non-mevalonate isoprenoid pathway. Cell. Mol. Life Sci. 68, 3797–3814.
[11] Rohdich, F. et al. (2002) Studies on the non-mevalonate terpene biosynthetic pathway: metabolic role of IspH (LytB) protein. Proc. Natl. Acad. Sci. USA 99, 1158–1163.
[12] Rekittke, I. et al. (2008) Structure of (*E*)-4-hydroxy-3-methyl-but-2-enyl diphosphate reductase, the terminal enzyme of the non-mevalonate pathway. J. Am. Chem. Soc. 130, 17206–17207.
[13] Grawert, T., Rohdich, F., Span, I., Bacher, A., Eisenreich, W., Eppinger, J. and Groll, M. (2009) Structure of active IspH enzyme from *Escherichia coli* provides mechanistic insights into substrate reduction. Angew. Chem., Int. Ed. Engl. 48, 5756–5759.
[14] Grawert, T., Span, I., Eisenreich, W., Rohdich, F., Eppinger, J., Bacher, A. and Groll, M. (2010) Probing the reaction mechanism of IspH protein by X-ray structure analysis. Proc. Natl. Acad. Sci. USA 107, 1077–1081.
[15] Wang, W., Li, J., Wang, K., Smirnova, T.I. and Oldfield, E. (2011) Pyridine inhibitor binding to the 4Fe–4S protein *A. aeolicus* IspH (LytB): a HYSCORE investigation. J. Am. Chem. Soc. 133, 6525–6528.
[16] Rohrich, R.C. et al. (2005) Reconstitution of an apicoplast-localised electron transfer pathway involved in the isoprenoid biosynthesis of *Plasmodium falciparum*. FEBS Lett. 579, 6433–6438.
[17] Kabsch, W. (1993) Automatic processing of rotation diffraction data from crystals of initially unknown symmetry and cell constants. J. Appl. Crystallogr. 26, 795–800.
[18] Schneider, T.R. and Sheldrick, G.M. (2002) Substructure solution with SHELXD. Acta Crystallogr. D Biol. Crystallogr. 58, 1772–1779.
[19] Vonrhein, C., Blanc, E., Roversi, P. and Bricogne, G. (2007) Automated structure solution with autoSHARP. Methods Mol. Biol. 364, 215–230.
[20] Abrahams, J.P. and Leslie, A.G. (1996) Methods used in the structure determination of bovine mitochondrial F1 ATPase. Acta Crystallogr. D Biol. Crystallogr. 52, 30–42.
[21] Emsley, P. and Cowtan, K. (2004) Coot: model-building tools for molecular graphics. Acta Crystallogr. D Biol. Crystallogr. 60, 2126–2132.
[22] Murshudov, G.N., Vagin, A.A. and Dodson, E.J. (1997) Refinement of macromolecular structures by the maximum-likelihood method. Acta Crystallogr. D Biol. Crystallogr. 53, 240–255.
[23] Abagyan, R. and Totrov, M. (1994) Biased probability Monte Carlo conformational searches and electrostatic calculations for peptides and proteins. J. Mol. Biol. 235, 983–1002.
[24] Fernandez-Recio, J., Totrov, M., Skorodumov, C. and Abagyan, R. (2005) Optimal docking area: a new method for predicting protein–protein interaction sites. Proteins 58, 134–143.
[25] Holm, L. and Sander, C. (1993) Protein structure comparison by alignment of distance matrices. J. Mol. Biol. 233, 123–138.
[26] Grawert, T. et al. (2004) IspH protein of *Escherichia coli*: studies on iron–sulfur cluster implementation and catalysis. J. Am. Chem. Soc. 126, 12847–12855.